New Journal of Physics
An Institute of Physics and Deutsche Physikalische Gesellschaft Journal

Examples for application and diagnostics in plasma–powder interaction

H Kersten[1], R Wiese[2], G Thieme[2], M Fröhlich[2], A Kopitov[2], D Bojic[2], F Scholze[3], H Neumann[3], M Quaas[4], H Wulff[4] and R Hippler[2]

[1] Institute for Nonthermal Plasmaphysics (INP), F-L-Jahn-Straße 19, D-17489 Greifswald, Germany
[2] Institute for Physics, University of Greifswald, Domstrasse 10a, D-17487 Greifswald, Germany
[3] Institute for Surface Modification (IOM), Permoserstrasse 15, D-04318 Leipzig, Germany
[4] Institute of Chemistry and Biochemistry, University of Greifswald, Soldmannstraße 16/17, D-17487 Greifswald, Germany
E-mail: kersten@inp-greifswald.de

New Journal of Physics **5** (2003) 93.1–93.15 (http://www.njp.org/)
Received 21 May 2003
Published 15 July 2003

Abstract. Low-pressure plasmas offer a unique possibility of confinement, control and fine tailoring of particle properties. Hence, dusty plasmas have grown into a vast field and new applications of plasma-processed dust particles are emerging. There is demand for particles with special properties and for particle-seeded composite materials. For example, the stability of luminophore particles could be improved by coating with protective Al_2O_3 films which are deposited by a PECVD process using a metal-organic precursor gas.

Alternatively, the interaction between plasma and injected micro-disperse powder particles can also be used as a diagnostic tool for the study of plasma surface processes. Two examples will be provided: the interaction of micro-sized (SiO_2) grains confined in a radiofrequency plasma with an external ion beam as well as the effect of a dc-magnetron discharge on confined particles during deposition have been investigated.

1367-2630/03/000093+15$30.00
PII: S1367-2630(03)63702-X

Contents

1. Introduction

Interest in the field of plasma–particle interaction with respect to dusty plasmas has grown enormously over the past decade. At present, this interest is due to applied research related to material science and surface-processing technology [1]–[3] and recently has also been with respect to plasma diagnostics [4]–[6].

There are several links between dusty plasma physics and material science. The trend is similar to the well-established plasma surface modification technology, except that now the surface of dust particles is the subject of treatment. The aim is to tailor particle properties for specific purposes. Here one can think of deposition, etching, surface activation, modification or separation of clustered grains in the plasma. In these types of processing, particles are either grown in the plasma or they are externally injected for subsequent treatment. The size, structure and composition of the grains can be tailored to specific requirements, dependent on the desired application. For example, one approach for coating externally injected toner particles has been demonstrated in [7]. An argon radiofrequency (rf) plasma was employed to charge and confine particles, while a metal coating was performed by means of a separate dc-magneteron sputter source.

The various plasma–powder technologies include:

- the treatment of soot and aerosols for environmental protection;
- particle synthesis in high- and low-pressure plasmas;
- the enhancement of adhesive, mechanical and protective properties of powder particles for sintering processes in metallurgy;
- fragmentation of powder mixtures to sort them;
- improvement of thin film properties by the incorporation of nanocrystallites for amorphous solar cells and hard coatings;
- coating of lubricant particles;
- functionalization of micro-particles for pharmaceutical and medical applications;
- the production of colour pigments for paints;
- surface protection of phosphor particles for fluorescent lamps or electroluminescent panels;
- the tailoring of optical surface properties of toner particles;
- application of processed powder particles for chemical catalysis; and
- the use of particles for diagnostics.

In this paper, we present new examples of the technological application of plasma powder treatment and of the use of dust grains as diagnostic tools in process plasmas. Firstly, phosphor particles have been coated by a protective alumina layer in a gas discharge containing a metal-organic precursor. The deposited layer shall protect the individual phosphor particles against degradation and ageing during plasma and UV irradiation in fluorescent lamps.

Secondly, examples of plasma process technology related to the interaction of micro-sized (SiO_2) grains confined in an rf plasma with an external ion beam as well as the effect of a dc-magnetron discharge on confined particles will be described in the paper. The interaction between plasma and injected micro-disperse powder particles can also be used as a diagnostic tool for the characterization of:

- electric fields in the plasma sheath (particles as electrostatic micro-probes) [8];
- energy fluxes in the plasma and towards surfaces (particles as micro-calorimeters) [5, 9]; and
- plasma–wall interaction (particles as micro-substrates) [10].

By observing the position and movement of the particles dependent on the discharge parameters, information can be obtained on the electric field and the electric potential distribution in front of electrodes and substrate surfaces where other plasma diagnostic methods fail. For instance, powder particles can be used as a kind of electrostatic micro-probe for the determination of plasma parameters.

2. Experimental details

Owing to the fact that rf technology is widely used in industry, and because it has been extensively shown that powder particles injected into such a plasma can be efficiently charged and trapped, an asymmetric, capacitively coupled rf discharge was used. The experiments have been performed in the reactor PULVA1, which is schematically drawn in figure 1. The plasma glow is located in the region between the planar aluminium rf electrode ($D = 130$ mm) and the upper part of the spherically shaped reactor vessel ($D = 400$ mm) which serves as a grounded electrode. The 13.56 MHz rf power is supplied by a generator (Dressler CESAR1310) in combination with an automatic matching network (Dressler VM700). The rf voltage was varied between 200 and 900 V, resulting in a discharge power of 5–100 W. The turbopump Pfeiffer TMU260C which allows for a base pressure of 10^{-4} Pa is connected to the vessel by a butterfly valve, the gas pressure was varied between 0.5 and 20 Pa by the valve and by using a flow controller (MKS). Argon, air and aluminium-tri-isopropyloxide (ATI), respectively, were used as the process gases.

The plasmas of the rf discharge as well as the ion beam and magnetron discharge have been studied by several diagnostics. Langmuir-probe measurements and self-excited electron resonance spectroscopy (SEERS, ASI Hercules) [11] provided information on the electron component, whereas a thermal probe was used for the determination of the energy influx towards the particles [12, 13]. Analytical CCD photometry (SBIG ST-6) and video recording (TELI CF8320BC) were employed to obtain information on the powder particles distributed in the plasma and illuminated by a laser fan at 532 nm (Spectra Physics Millenia V).

In the (first) coating experiment, the metal-organic precursor ATI has been dissociated in the rf discharge containing an ATI/Ar or ATI/air mixture, respectively. The rf power has been varied between 10 and 100 W and the gas flow rate between 0.5 and 10 sccm. Changes in

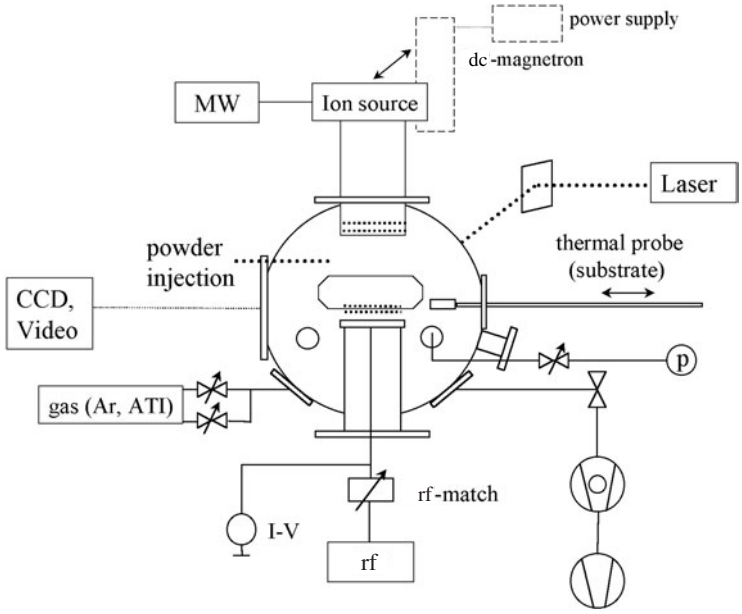

Figure 1. Schematic of the experimental set-up. The ion beam source on top of the reactor could be replaced by a magnetron sputter source.

the electron density during the process have been measured by SEERS. After decomposition of the ATI ($Al(i\text{-}OC_3H_7)_3$) precursor thin alumina films have been deposited surrounding the injected phosphor particles proved by x-ray photoelectron spectroscopy (XPS). The particles are high-brightness, high-maintenance phosphors often used as the blue component in a tricolour fluorescent lamp which consists of $BaMg_2Al_{16}O_{27}:Eu^{2+}$.

In the second experiment, where the interaction of an external ion beam with confined powder particles was studied, the ion source was mounted on top of the vacuum chamber, see figure 1. The ion beam source (IOM EC/A 125 [14]) was supplied with power of about 130 W by a generator (Aalter SM 445) via a microwave antenna. At 87.5 mT and 2.4 GHz the electrons are strongly accelerated by the electron cyclotron resonance and ionize the argon atoms. The generated ions are extracted by a graphite grid system (diameter: 125 mm) and accelerated by the beam voltage which was varied between 200 and 700 V. An additional turbopump (Leybold) allows for gas pressures between 10^{-2} and 10^{-1} Pa even at high flow rates (3, 10 sccm) which are necessary for the operation of the ion gun.

Whereas the mean plasma density in the confining rf plasma is of the order of 2×10^8 cm^{-3}, the external ion beam supplies an additional energetic ion flux of about 300 μA cm^{-2} which interacts with the particle cloud. The beam profile could be visualized by the interaction of the ion beam with the micro-disperse particles, which have been charged and confined in the weak rf plasma (5–20 W) in front of the electrode within a region of a circular potential trap formed by a ring. The distance of the particles to the ion source was about 210 mm. The spatial distribution of the injected SiO_2 ($\sim$1 μm) particles in the rf-plasma sheath during ion beam operation was also compared with the beam profile obtained by thermal probe measurements across the beam.

Finally, in the third experiment the ion source was removed and replaced by a dc-magnetron source (von Ardenne PPS 50) opposite the rf electrode. Typical experimental conditions were: pressure 3–20 Pa, rf power 1–10 W, magnetron power 10–200 W supplied by a generator

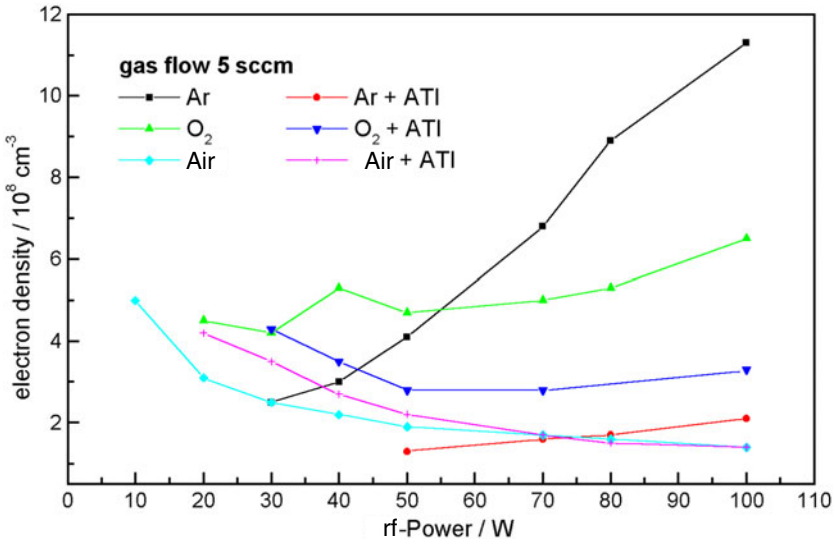

Figure 2. Electron density as measured by SEERS with respect to dependence on discharge power.

(Advanced Energy MDX 500). For these experiments silicon oxide particles with a diameter of 18 μm were used. The particles were again trapped in the sheath above the rf electrode. In order to confine the particles in the centre a copper ring was again placed on the rf electrode. The planar dc-magnetron sputter source mounted on top of the reactor was used to deposit thin metallic films on the particles which served as micro-substrates. As targets Al-, Cu- or Ti-cathodes, respectively, were taken. The distance between the target and the trapped particles was about 70 mm.

3. Results and discussion

3.1. Deposition of protective coatings on individual phosphor particles

An example of technological powder treatment in process plasma is the deposition of alumina coatings on individual phosphor particles by a PECVD process. The deposited layers protect the particles against degradation and ageing during plasma and UV irradiation in fluorescent lamps. Thin films of alumina (Al_2O_3) are chemically stable and allow a substantially full light transmission at the excitation wavelength of mercury (254 nm) and in the visible range.

As original material the aluminium-organic precursor ATI was used. The ATI molecules are dissociated in the rf-plasma volume and the radicals contribute to the formation of Al-oxide on the small phosphor particle substrates. Fragmentation and deposition essentially depend on the plasma parameters and the process cycle.

Owing to the fact that the ATI fragments tend to form negative ions the electron density shows only a weak variation with the power, whereas in a pure argon plasma a strong increase could be observed (figure 2). This observation is due to the electron attachment by the radicals which contribute to the film growth at the luminophore particles. In a pure argon plasma the electron density increases with increasing power (30–100 W) from 2×10^8 to 12×10^8 cm^{-3}, while the density in an Ar/ATI plasma is about 10^8 cm^{-3}. In the argon plasma the degree of ionization

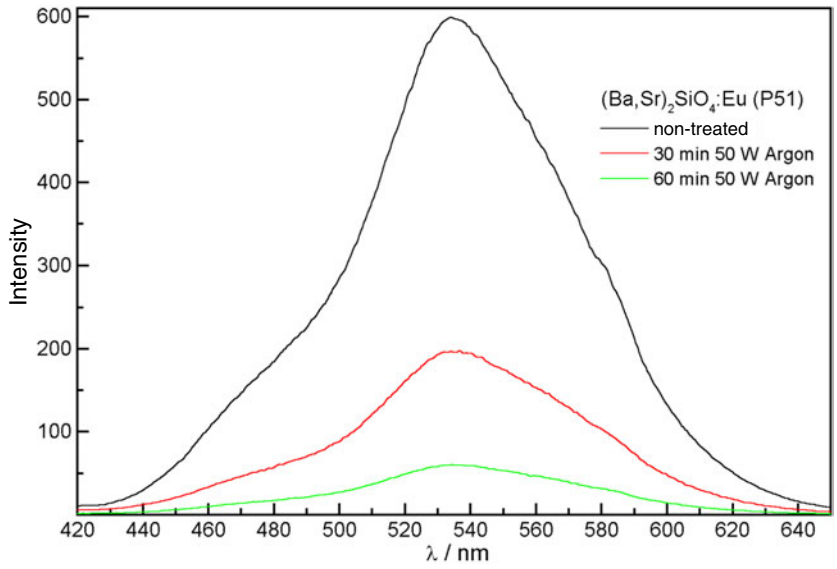

Figure 3. Spectral light intensity of non-treated luminophores after plasma irradiation.

increases with the discharge power and, hence, the density of the Ar^+ ions and electrons also increases. In ATI or O_2 plasma, respectively, the ionization also increases as a function of the discharge power. However, to a certain extent the electrons are attached at the radicals to form negative ions. As a result, the density of the free electrons almost does not change, see figure 2. The different order of magnitude and the tendency in the electron densities for different process conditions allow us to make conclusions about the dissociation and ionization mechanisms and reveals information about the thin film deposition on the fluorescent grains.

The original phosphor particles, which are not coated by a protective alumina layer, show a remarkable decrease in their light intensity after argon plasma treatment, which simulates the process conditions in a lamp (figure 3). Irradiating the plasma for 1 h at 50 W causes an ageing effect and a decrease in the light intensity of the luminophores by a factor of 10. Therefore, the particles have been coated by the protective alumina layer. The success of particle deposition was proved by XPS. It could be demonstrated that the luminophore grains show CH-groups from the glue before deposition, whereas almost no CH-groups could be detected by XPS on the particles after deposition of the protective layer. In comparison to the non-treated particles, PECVD decomposition of ATI in the rf plasma giving transparent Al_2O_3 films onto phosphor particles results in a much higher stability against plasma irradiation, e.g. against UV radiation and particle bombardment at low energies. Whereas the light intensity of non-treated luminophores decreases with high-power plasma irradiation, the light intensity of coated luminophores remains stable even for high power, see figure 4.

As the fluorescent properties of the grains should be preserved, it is important that there is no change in the emission spectra of the particles with respect to the Al_2O_3 protective layers. It can be shown that the emission spectra of alumina-coated $BaMg_2Al_{16}O_{27}:Eu^{2+}$ does not differ from that of the uncoated materials. An additional advantage of plasma treatment under optimized conditions (e.g. 30 W, 5 sccm air/ATI, 30 min treatment time) is the decomposition of the glue material, which makes any additional annealing processes unnecessary.

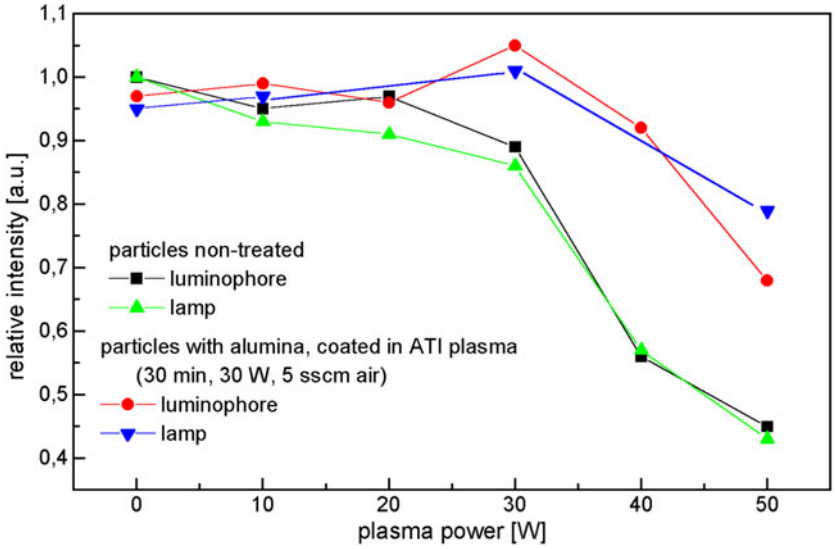

Figure 4. Comparison of light intensities of non-coated and coated luminophore particles after plasma irradiation.

3.2. Interaction of an external ion beam with confined dust grains

Ion beam technology has come of age over the past decade. For example, ion beam sources are widely used in sputtering, etching and smoothing of surfaces. Recently, the employment of ion beam sources as thrusters in space technology and as powerful tools in processing highly accurate optical lenses has received much attention. An important issue in this field is the development of broad ion beam sources which are used, for example, in the processing of large substrate surfaces [15, 16].

An essential requirement for new applications of ion beam technology is the desired tailoring of the beam profile. For optimization and adjustment, knowledge of the physical beam parameters and plasma processes in the ion source is necessary. Thus, the determination of the beam profile and the energy flux from the ion source towards the substrate surface during operation is of special interest [17].

The deposited power, which has been measured by a simple thermal probe [13], mainly depends on the beam voltage supplied, V_{beam}, assuming that the mean free path length of the ions in the residual gas is larger than the distance between the ion source and substrate. In this case, the energy influx J_{in} is the product of the ion current density j_{i} times the kinetic energy of the ions (E_{ion}) which is given by the difference in the beam voltage and the constant substrate voltage of the thermal probe. In addition, the ion current j_{i} was kept nearly constant, since the operation of the ion source was in the saturation regime where j_{i} is only affected by the discharge power of the source and not by the extracting beam voltage.

In the range considered here ($V_{\mathrm{beam}} = 100$–700 V), the deposited power J_{in} increases nearly linearly ($J_{\mathrm{in}} = 0.05$–0.45 J cm^{-2} s^{-1}) with applied beam voltage due to the increasing kinetic energy of the ions [18]. The influence of the beam voltage on the profile of the ion beam has also been studied. As an example, the profiles obtained at two different beam voltages (300, 700 V) are shown in figure 5. On comparing the two profiles at an argon gas flow of 3 sccm (10^{-2} Pa) it is obvious that at the edge of the ion beam at higher voltages the energy flux is almost double due to the higher divergence of the beam. However, at a higher gas flow of 10 sccm this effect

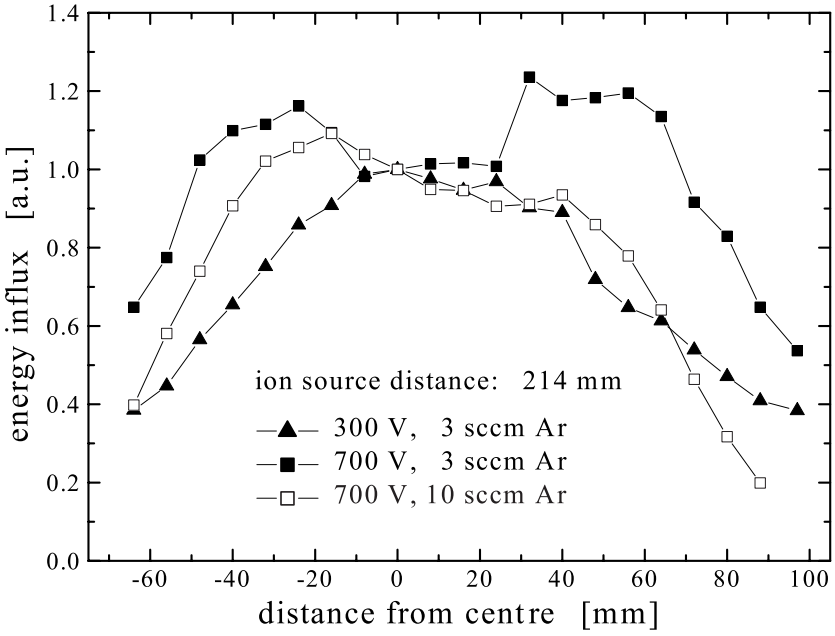

Figure 5. Influence of beam voltage and gas flow on the profile of the energy influx (deposited power).

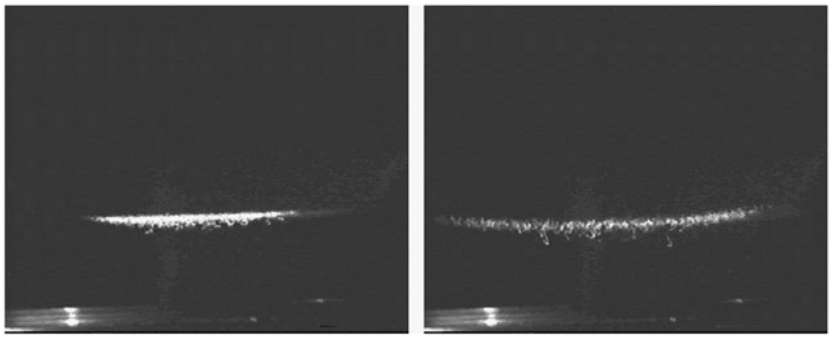

Figure 6. Confined dust particles in the rf plasma without (a) and with (b) beam operation.

is compensated by an increasing number of ion collisions at higher gas pressure (10^{-1} Pa). The 'amplification' of the edge regions under certain conditions can be regarded as an improvement in the homogeneity across the broad beam.

Additionally, the ion beam profile was visualized by small dust particles which are levitated in front of the rf electrode (figure 6(a)). If the beam is switched on, the shape of the particle cloud is changed in a characteristic manner (figure 6(b)) reflecting the beam operation.

Charging, confinement and movement of the dust particles are essentially influenced by the presence of additional electric fields and forces onto the particles which are provided in our experiments by the external ion beam in order to simulate the influence of ions in a complex plasma.

The dependence of the measured height of the dust particle cloud above the rf electrode on the ion beam voltage is plotted in figure 7. For small beam voltages ($V_{\mathrm{beam}} < 200$ V) there is almost no influence. Due to a variation in the sheath width, which is influenced by gas pressure

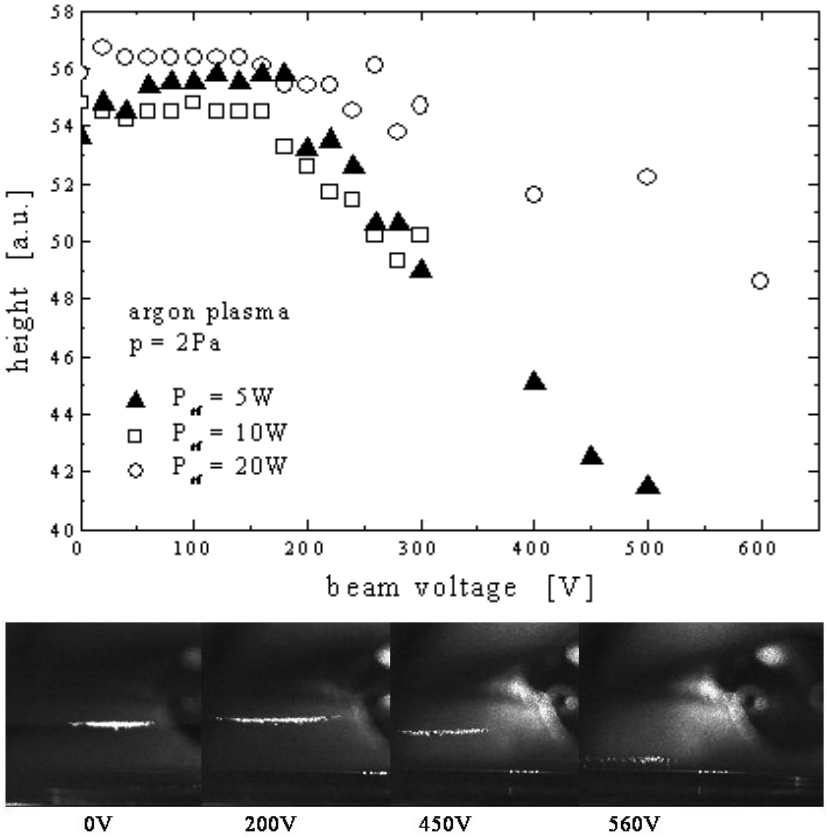

Figure 7. Particle cloud in front of the rf electrode at different ion beam voltages, and the measured height of the particles.

and rf power, the trapped particles only follow the variations in the rf plasma. The beam voltage is not sufficiently high enough to extract a remarkable number of ions into the dust region which is about 210 mm away from the grid system of the ion source. When the beam voltage increases, the height of the dust particles decreases. That means the originally planar dust cloud forms a parabolic shape and moves into the direction of the rf electrode. For higher powers of the rf plasma and, hence, for higher bias voltage of the electrode the particle cloud is levitated in a higher position than for smaller rf powers. This observation is due to the electric field (potential) in front of the powered rf electrode. At higher bias voltages, the field can compensate for the influence of the external ion beam more efficiently (figure 7).

As the additional ion supply by the external ion beam interacts with the rf plasma, the plasma density in the trapping region is changed. This effect causes a variation in the sheath (width and shape) and, thus, a variation in the force balance of the particles. Another effect of the additional ion flux is an enhanced charge carrier recombination at the surface of the negatively floating dust grains. It can be expected that the net charge is decreased by recombination. Ion bombardment also leads to additional heating of the particles. Certainly, the ion drag force created by the ions of the beam also influences the force balance of the confined grains. The importance of this effect has often been discussed with respect to the void formation in plasma crystals [19, 20].

By varying the experimental conditions, one of the three effects mentioned above may be dominant, e.g. varying the discharge power, beam voltage, pressure or particle size. Assuming

that there would only be a weak change in the electric field shape in front of the rf electrode and almost no influence on the particle charge during beam operation, the change in the position of the particles could only be caused by the ion drag.

Under these conditions, the electrostatic force has to compensate for the sum of gravitation and ion drag. The electrostatic force F_{el} is given by the product of the particle charge Q times the electric field strength $E(z_0)$ at the trapping position z_0. The field was in the order of 3×10^3 V m^{-1} and the charge was about $2 \times 10^3\, e_0$. The gravitational force F_G depends on the mass m of the particles which was 2×10^{-15} kg. This simplified model assumption finally results in an ion beam drag force of about 10^{-12} N (at $V_{beam} = 500$ V) which is larger than the gravitational force and which has to be balanced by the electrostatic force due to the electric field in the rf sheath.

To summarize, it can be seen that by visualization of the shape of confined dust particles in combination with other diagnostic methods (e.g. energy flux measurements) the profile of an ion beam can be suitably characterized.

3.3. Coating of powder particles in a magnetron discharge

Thin metallic films (Al, Ti, Cu) were deposited by means of dc-magnetron sputtering on silicon oxide particles (18 μm in diameter) suspended in the argon rf discharge (5 Pa, 5 W). The coated particles were examined by electron microscopy (SEM). Some pictures of the particles are shown in figure 8.

The structure of the metallic films was different depending on the target material. While the Al- and Cu-films were deposited smoothly, the Ti-films showed a distinct island formation. This can be explained by the lower sputter yield of the titanium target and also by the different surface adhesion between the particles and the deposited material [21]. The surface energy of titanium (1.39 J m^{-2}) is higher than that of aluminium (0.91 J m^{-2}) and copper and, therefore, the wetting of the particle surface is worse for titanium.

The deposition rates have been determined as a function of the magnetron power. To obtain the film thickness the metals were sputtered pre-experimentally onto glass substrates. During the deposition process the transmission of the sample was determined and, by taking into account the optical relationships, the thickness and, thus, the growth rate could be estimated. In conclusion, from the parameter study of the deposition rate at the relevant experimental conditions (magnetron power between 30 and 100 W) one can expect growth rates of 0.5–2.5 nm s^{-1} for aluminium and titanium layers and growth rates of 2.5–15 nm s^{-1} for copper on the powder grains. This expectation is also supported by observation of the surrounding films on the powder particles, see for example figure 8(d). These are rather reliable values which satisfy the requirements of the applications well. For an optically thick aluminium coating of about 60 nm the particles have to be confined for 1 minute, which is not a problem because the particles can be trapped for hours.

The difference between the original and powder-coated particles is obvious. The particles are completely covered with close and quite thick metal layers. The coated particles show a rough and cauliflower-like shape which makes them attractive, especially for catalytic applications. The modified particles also differ from the originals in their contrast. If the deposited films were thinner, the layer surrounding the particles could also be smoother. In such cases the surface structure of the coated particles (which was still completely closed) looked more golfball-like which might be interesting for optical applications.

In the experimental set-up used it was only possible to trap about 10^5 particles per cubic centimetre. This corresponded to a mass of about 0.5 mg. The particles were treated in the magnetron discharge for about 5 minutes. The metallic layers were deposited evenly on all the

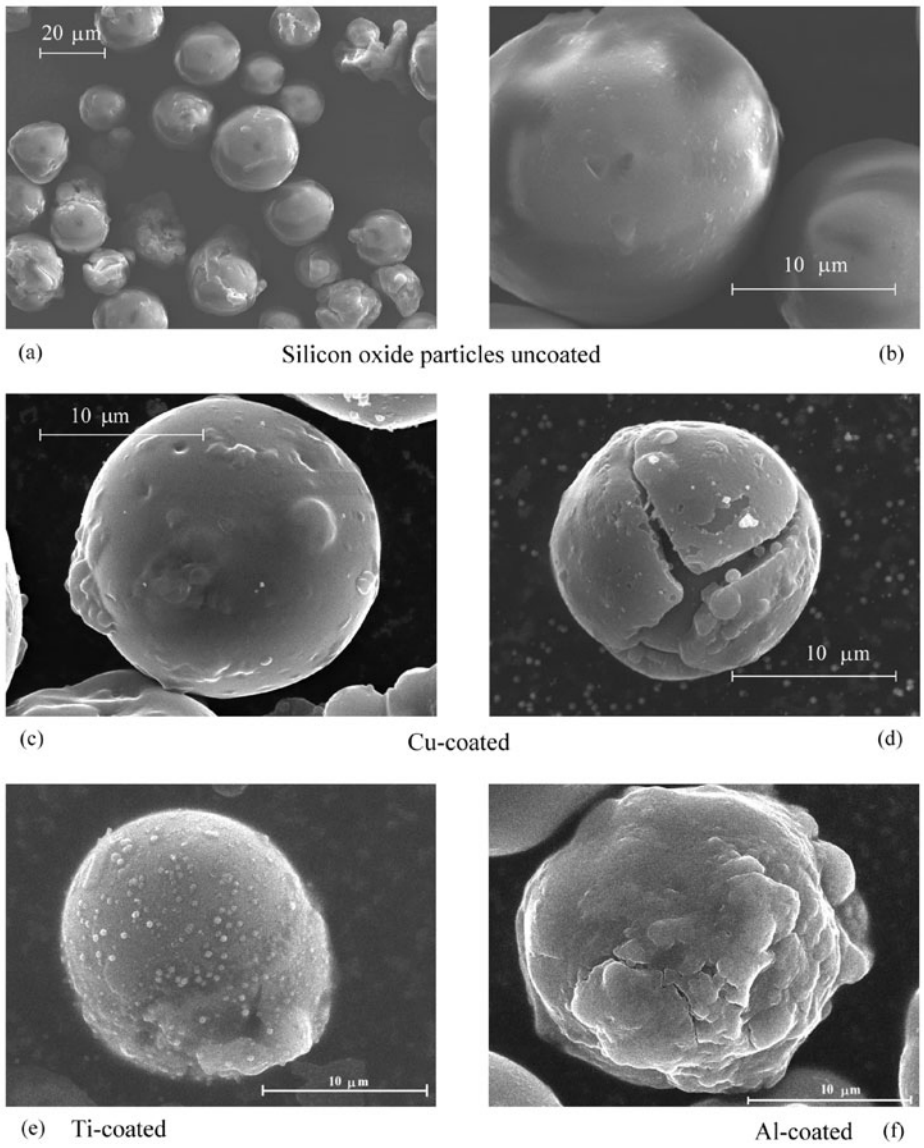

Figure 8. SEM photographs of silicon oxide particles coated by magnetron sputtering.

particles. This would give a yield of coated particles of about 50 mg h^{-1} if it were possible to extract the particles directly from the reactor through some kind of load–lock system. This is not very much but can probably be enhanced using a scaled set-up.

During the magnetron experiments, an interesting observation was made: when the magnetron was turned on the entire particle cloud began to rotate, see figure 9. After the magnetron was turned off the rotation ceased due to the neutral drag. Similar observations of particle motion under the influence of a permanent magnetic field were made by Konopka *et al* [22]. They explain the rotation with the azimuthal component of the ion drag force as being due to $\boldsymbol{E} \times \boldsymbol{B}$-drift of the ions in the perpendicular radial electric and vertical magnetic fields.

However, we observed particle cloud rotation only under the influence of magnetron discharge. This means that for this effect the interaction of the rf plasma and the magnetron discharge is of significance.

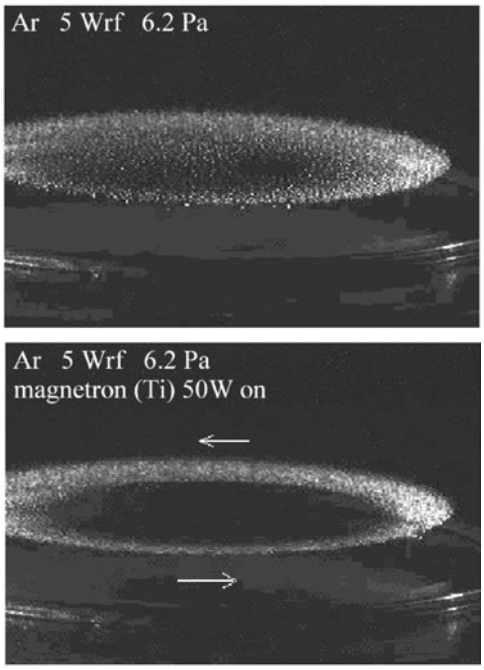

Figure 9. Particle cloud before and after the magnetron was turned on.

The magnetic field of the permanent magnets in the magnetron is already very weak for this particle distance ($B_{z,\mathrm{Mag}} \approx 10^{-4}$ T). It alone has no impact on the particles. Thus, we believe that the electrons (which exist under high density due to the magnetron effect in front of the target cathode) must be responsible for the ion drift. With these circulating electrons an additional magnetic field is formed and an additional electron current in the direction of the opposite rf electrode is supplied. This current was observed in earlier experiments.

We ascribe the rotation of the particle cloud to an $\boldsymbol{E} \times \boldsymbol{B}$-drift of the argon ions which interact through impulse transfer with the particles. The perpendicular fields responsible for the ion drift are the vertical component of the permanent magnetic field, $B_{z,\mathrm{Mag}}$, of the magnetron and the radial components of the electric field above the rf electrode which is changed significantly by the influence of the magnetron plasma particularly through the flow of electrons from the magnetron plasma (figure 10). Finally, the momentum transfer of the ions (ion drag) due to the tangential Lorentz force causes the grains to rotate. Even if the ion drag is only just sufficient in a small circular region, the other dust particles are coupled to each other by Coulomb interaction [23]. This also explains why the entire particle cloud rotates like a rigid solid with the same frequency.

The motion of the particle cloud was studied using different parameters. Figure 11 shows the rotation frequency as a function of the magnetron power. It increases linearly with increasing magnetron power accounting for the increase in the charge carrier density in the magnetron discharge. This observation supports our supposition on the influence of the interaction with the electron ring current, since the density of the charge carriers increases with the magnetron discharge power. The dependence on the gas pressure was also studied (figure 12). The rotation frequency f_{rot} decreases with as the pressure p increases which can be explained by the neutral friction force F_{N} increasing (neutral drag).

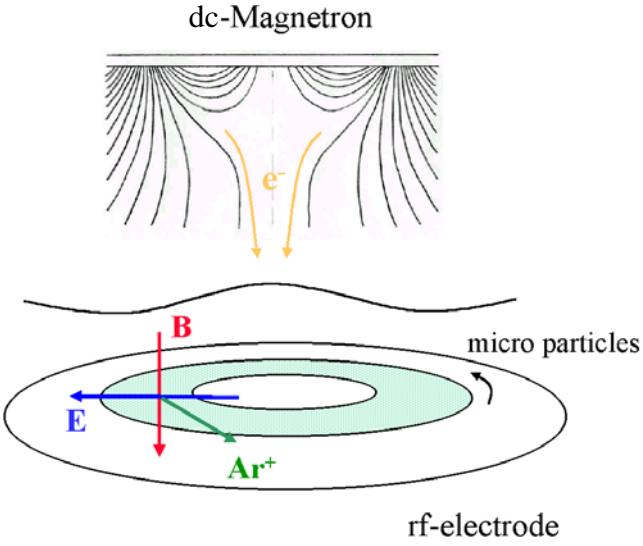

Figure 10. Principle sketch of the fields which cause (by the tangential ion drag) the rotation of the grains with magnetron operation.

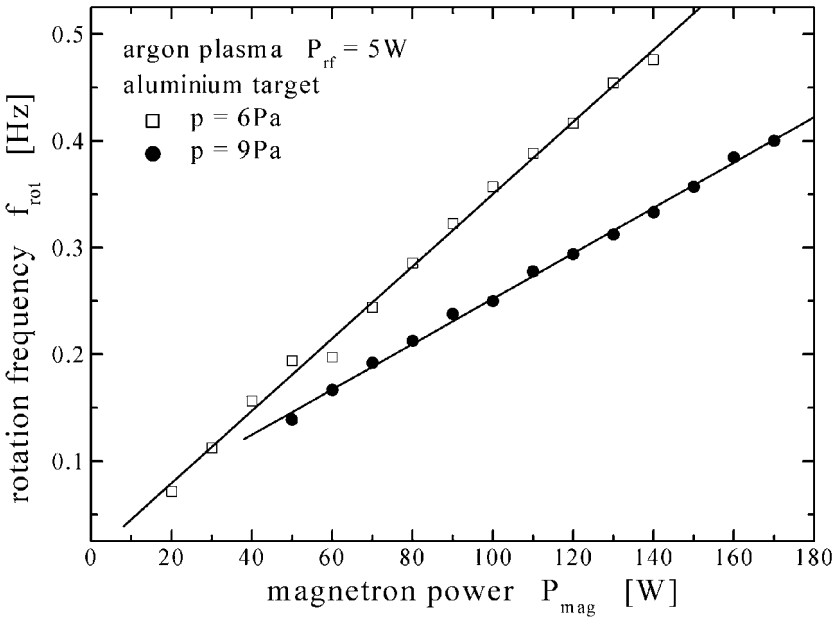

Figure 11. Rotation frequency of the particle cloud as a function of the magnetron power at different gas pressures.

For the rotation frequency the force balance between the ion drag F_{ion} and the neutral drag F_{N} is important [24]

$$F_N = \xi p v_S = F_{\text{ion}}$$

where p is the gas pressure, $v_S = 2\pi r_S f_{\text{rot}}$ is the rotation velocity of the particle cloud, r_S is the mean radius of the rotating particle ring and ξ is a constant.

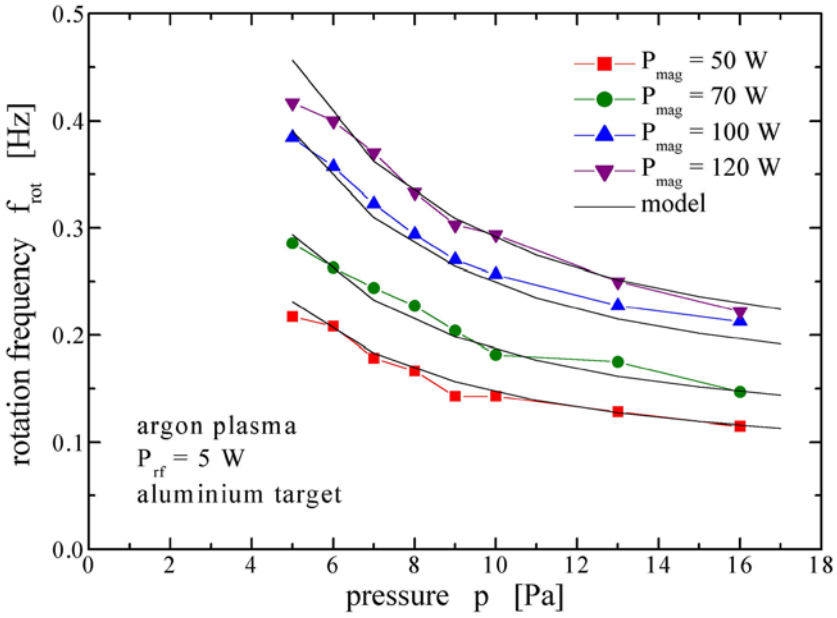

Figure 12. Pressure dependence on the particle cloud rotation frequency at different powers.

With this we can derive the following expression for the rotation frequency [25, 26]:

$$f_{\mathrm{rot}} = \frac{(\sigma_{\mathrm{coll}} + \sigma_{\mathrm{coul}})n_{\mathrm{i}}(p,\, P_{\mathrm{mag}})m_{\mathrm{Ar}}v_{\mathrm{di}}\sqrt{v_{\mathrm{di}}^2 + v_{\mathrm{th,i}}^2}}{2\pi r_S \xi}\frac{1}{p}$$

where σ_{coll} is the collision cross section for ion momentum transfer, σ_{coul} is the cross section for Coulomb interaction, n_{i} is the ion density, m_{Ar} is the ion mass, v_{di} is the drift velocity of the ions and $v_{\mathrm{th,i}}$ is the thermal velocity of the ions.

Figure 12 shows a comparison of the experimental data points and the model. The curve yields a friction force of about 5×10^{-13} N which is of the same order as the confining forces.

4. Conclusion

Powder trapping, modification and coating in laboratory discharges have been subjects of growing interest over the past decade. There are possibilities for coating powder particles for technological applications as has been demonstrated.

In the initial experiment, luminophore grains were coated by a protective alumina layer in a metal-organic PECVD process. The treated particles showed better stability in their light intensity, meaning that the surface properties with respect to degradation by plasma irradiation could be remarkably improved. Furthermore, small SiO_2 grains were coated by thin metallic films with a combined plasma configuration of an rf plasma for particle charging and trapping, and a dc-magnetron sputter source for deposition. However, the number of the confined particles and, thus, the yield of the modified powder is still rather small and must be increased for reasonable industrial application.

The interaction between process plasma and injected micro-disperse powder particles can also be used as a diagnostic tool for the study of plasma surface mechanisms in low-pressure plasmas. For example, with magnetron sputtering of thin films onto dust grains the observation

and interpretation of the particle cloud rotation under the influence of a magnetron discharge reveals information on the electron flux pattern as well as on the neutral and ion drag. The effect of the ion drag was also studied during the interaction of an external ion beam source with confined dust particles in another experiment. In combination with other diagnostic methods (e.g. energy flux measurements), by visualizing the shape of the confined dust particles the profile of the ion beam can be suitably characterized to optimize the beam performance.

The examples presented emphasize that the technological application of complex plasmas is a promising field of research in the frontier between plasma physics, material processing and diagnostics.

Acknowledgments

This work has been partly supported by the Deutsche Forschungsgemeinschaft (DFG) under SFB198/A14 and the Bundesministerium für Bildung und Forschung (BMBF) under 13N7920. The authors gratefully acknowledge M Hähnel and A Knuth for their support.

References

[1] Selwyn G S, McKillop J S, Haller K L and Wu J J 1990 *J. Vac. Sci. Technol.* A **8** 1726
[2] Bouchoule A (ed) 1999 *Dusty Plasmas: Physics, Chemistry and Technological Impacts in Plasma Processing* (New York: Wiley)
[3] Stoffels E, Stoffels W W, Kersten H, Swinkels G H P M and Kroesen G M W 2001 *Phys. Scr.* T **89** 168
[4] Law D A, Tomme E B, Steel W H, Anaratonne B M and Allen J E 1999 *Proc. XXIV ICPIG (Warsaw, Poland, 1999)* Proc. IV/109
[5] Swinkels G H P M, Kersten H, Deutsch H and Kroesen G M W 2000 *J. Appl. Phys.* **88** 1747
[6] Kersten H, Deutsch H, Stoffels E, Stoffels W W and Kroesen G M W 2003 *Int. J. Mass Spectr.* **223/224** 313
[7] Kersten H, Schmetz P and Kroesen G M W 1998 *Surf. Coat. Technol.* **108/109** 507
[8] Tomme E B, Law D A, Annaratone B M and Allen J E 2000 *Phys. Rev. Lett.* **85** 2518
[9] Daugherty J E and Graves D B 1993 *J. Vac. Sci. Technol.* A **11** 1126
[10] Kersten H, Deutsch H, Otte M, Swinkels G H P M and Kroesen G M W 2000 *Thin Solid Films* **377/378** 530
[11] Klick M 1996 *J. Appl. Phys.* **79** 3445
[12] Kersten H, Rohde D, Berndt J, Deutsch H and Hippler R 2000 *Thin Solid Films* **377/378** 585
[13] Kersten H, Deutsch H, Steffen H, Kroesen G M W and Hippler R 2001 *Vacuum* **63** 385
[14] Zeuner M, Neumann H, Scholze F, Flamm D, Tartz M and Bigl F 1998 *Plasma Sourc. Sci. Technol.* **7** 252
[15] Vukusic J, Bengtsson J, Ghisoni M, Larsson C, Carlstrom C F and Landgren G 2000 *Appl. Opt.* **39** 398
[16] Frost F, Lippold G, Otte K, Hirsch D, Schindler A and Bigl F 1999 *J. Vac. Sci.Technol.* A **17** 793
[17] Kersten H, Wiese R, Gorbov D, Kopitov A, Scholze F and Neumann H 2003 *Surf. Coat. Technol.* at press
[18] Kersten H, Stoffels E, Stoffels W W, Otte M, Csambal C, Deutsch H and Hippler R 2000 *J. Appl. Phys.* **87** 3637
[19] Mikikian M, Boufendi L, Bouchoule A, Thomas H M, Morfill G E, Nefedov A P, Fortov V E and the PKE-Nefedov team 2003 *New J. Phys.* **5** 19.1
[20] Thieme G, Wiese R, Gorbov D, Kersten H and Hippler R 2002 *Dusty Plasma in The New Millenium (AIP Proc. vol 649)* p 333
[21] Vollertsen F and Vogler S 1989 *Werkstoffeigenschaften und Mikrostruktur* (München: Hanser)
[22] Konopka U, Samsonov D, Ivlev A V, Goree J and Steinberg V 2000 *Phys. Rev.* E **61** 1890
[23] Klindworth M, Melzer A and Piel A 2000 *Phys. Rev.* B **61** 8404
[24] Epstein P S 1924 *Phys. Rev.* **23** 710
[25] Barnes M S, Keller J H, Foster J C, O'Neill J A and Coultas D K 1992 *Phys. Rev. Lett.* **68** 313
[26] Kilgore M D, Daugherty J E, Porteous R K and Graves D B 1993 *J. Appl. Phys.* **73** 7195